J Nanopart Res (2012) 14:1148
DOI 10.1007/s11051-012-1148-2

RESEARCH PAPER

Development of a gold-nanostructured surface for amperometric genosensors

Chiara Zanardi · Clara Baldoli · Emanuela Licandro · Fabio Terzi · Renato Seeber

Received: 15 March 2012 / Accepted: 23 August 2012

Abstract A gold-nanostructured surface has been obtained by stable deposition of chemically synthesized gold nanoparticles (2.1–5.5 nm size range) on a gold substrate through a dithiol linker. The method proposed for the obtainment of the nanostructure is suitable for the further stable anchoring of a peptide nucleic acid oligomer through four amine groups of lysine terminal residues, leading to fairly reproducible systems. The geometric area of the nanostructured surface is compared with those of a smooth and of an electrochemically generated nanostructured surface by depositing a probe bearing an electrochemically active ferrocene residue. Despite the area of the two nanostructures being quite similar, the response toward a 2 nM target oligonucleotide sequence is particularly high when using the surface built up by nanoparticle deposition. This aspect indicates that morphologic details of the nanostructure play a key role in conditioning the performances of the genosensors.

Keywords Gold nanoparticles · Nanostructured surface · Amperometric genosensor · Peptide nucleic acid · Ferrocene derivatives · Amine deposition

C. Zanardi (✉) · F. Terzi · R. Seeber
Dipartimento di Chimica, Università di Modena e Reggio Emilia, Modena, Italy
e-mail: chiara.zanardi@unimore.it

C. Baldoli (✉)
Istituto di Scienze e Tecnologie Molecolari del CNR, Milan, Italy
e-mail: clara.baldoli@istm.cnr.it

E. Licandro
Dipartimento di Chimica Organica ed Industriale, Università degli Studi di Milano, Milan, Italy

Introduction

The increasing request for early diagnosis of genetic diseases and infectious bacteria has led to the necessity of developing more sensitive screening tests based on DNA recognition. This forced the scientific community, on one hand, to synthesize highly efficient probes capable of discriminating among many different oligonucleotide sequences and, on the other hand, to put utmost effort to the development of nanomaterials (Wang 2005; Rosi and Mirkin 2005; Erdem 2007; Lord and Kelley 2009; Salah et al. 2010; Wang et al. 2011a; Li et al. 2012) capable of increasing the sensitivity of the resulting sensor.

When considering selectivity, the use of peptide nucleic acids (PNA) has proven to significantly improve the performance of the resulting genosensor due to the capability of this class of molecules to bind complementary DNA and RNA with higher affinity and selectivity than natural nucleic acids (Nielsen 2004). Therefore, they are suitable candidates for

Published online: 12 September 2012

hybridization-based applications and powerful tools for analytical and biotechnological applications (Oh and Choi 2010; Mateo-Martí and Pradier 2010; Sforza et al. 2011; Pournaghi-Azar et al. 2010; Fang and Kelley 2009; Hejazi et al. 2011). Since the electrochemical transducer generally consists of gold surfaces, due to its high affinity for many functional groups, functionalization of PNA molecules with thiol terminal groups has become a fundamental step in the development of many sensors. On the other hand, the possibility to use PNA derivatives containing amine residues significantly improves the solubility in water of this class of molecules (Vernille et al. 2004; Zanardi et al. 2012), making their deposition from aqueous solutions well feasible.

In order to improve the sensitivity of the sensor transduction, in many approaches, DNA strains under analysis are covalently bounded to gold nanoparticles (AuNPs) (Merkoçi 2010; Li et al. 2010). The occurrence of the hybridization is evidenced due to the consequent localization of AuNPs very close to the transducer surface; the recognition event is thus converted in an optical (D'Agata et al. 2010) or electrochemical (Castañeda et al. 2007) signal directly related to the amount of target nucleic acid.

On the other hand, the possibility to use label-free approaches represents a definite step forward in biosensors technology. Furthermore, as a very promising method proposed to improve the sensitivity of the device and to lower the limit of detection, nanostructured surfaces can be used as the anchoring platform for oligonucleotide probes (Fang and Kelley 2009; Fang et al. 2008; Cai et al. 2001; Gasparac et al. 2004; Soleymani et al. 2009; Soreta et al. 2011). The improved performances come out not only from the possibility to fix a higher number of molecular probes on the surface, but also to increase the accessibility of target oligonucleotide chains to the hybridization sites. This is a consequence of the small curvature radius of the surface from which the probes emerge (Cederquist and Keating 2009; Hill et al. 2009). Despite the great interest in nanostructured surfaces, the influence of the nanostructure morphology on the performances of the resulting device was only recently evidenced (Bin et al. 2010).

In the field of amperometric genosensors, gold-nanostructured surfaces are generally obtained through an electrochemical method, consisting of the reduction of $AuCl_4^-$ salt at a gold electrode, acting as the substrate, polarized at a suitable cathodic potential (Fang et al. 2008; Soreta et al. 2011; Ensafi et al. 2011; Wang et al. 2011b). Here, we show the advantages of using AuNPs (2.1–5.5 nm size range), that have been independently synthesized by the chemical route, for the construction of similar nanostructured surfaces. The synthesis of AuNPs has been carried out in order to surround them by a particularly labile encapsulating agent, such as chloride ion, that can be easily substituted by species-bearing functions with a higher affinity to Au, such as thiol and amine groups (Zanardi et al. 2012). The AuNPs have been stably fixed on the Au planar surfaces through a dithiol linker (Pasquali et al. 2007a, b, 2008, 2011). The performances of the nanostructured surface (Au_{NP}) thus obtained have been evaluated with respect to a bare, smooth surface (Au_{sm}) and to a nanostructured surface obtained through a widely diffused electrochemical approach (Au_{el}) (Fang et al. 2008; Ensafi et al. 2011; Carralero Sanz et al. 2005; Liu et al. 2005; Huang et al. 2008; Zhang et al. 2008). An electroactive probe—namely, *N*-(2-aminoethyl)-ferrocenecarboxyamide (FcCA in Fig. 1)—was used in order to compare the active area of the different Au surfaces and the reproducibility of gold nanostructure formation, which constitutes one of the most important aspects for genosensor application.

In order to study the behavior of the nanostructured surface with respect to anchoring amine groups, two further probes (Fig. 1) have been fixed on the Au surfaces: (1) a ferrocene-labeled tyrosine PNA monomer (FcPNAm) was used to test the effectiveness of the deposition of this particular PNA derivative on the developed Au_{NP} surface and (2) a homothymine PNA decamer bearing four lysine residues to the C-terminus, [PNA$(Lys)_4$], was finally used to test the efficiency of Au_{NP} surface for the construction of high performance amperometric genosensors.

Materials and methods

Reagents and apparatus

All reagents and solvents were obtained from commercial suppliers and used without further purification unless otherwise stated. Column chromatography was performed using Merck silica gel 60 (70–230 mesh). ^1H and ^{13}C NMR spectra were acquired on a Bruker AMX spectrometer at 300 MHz spectrometers; the

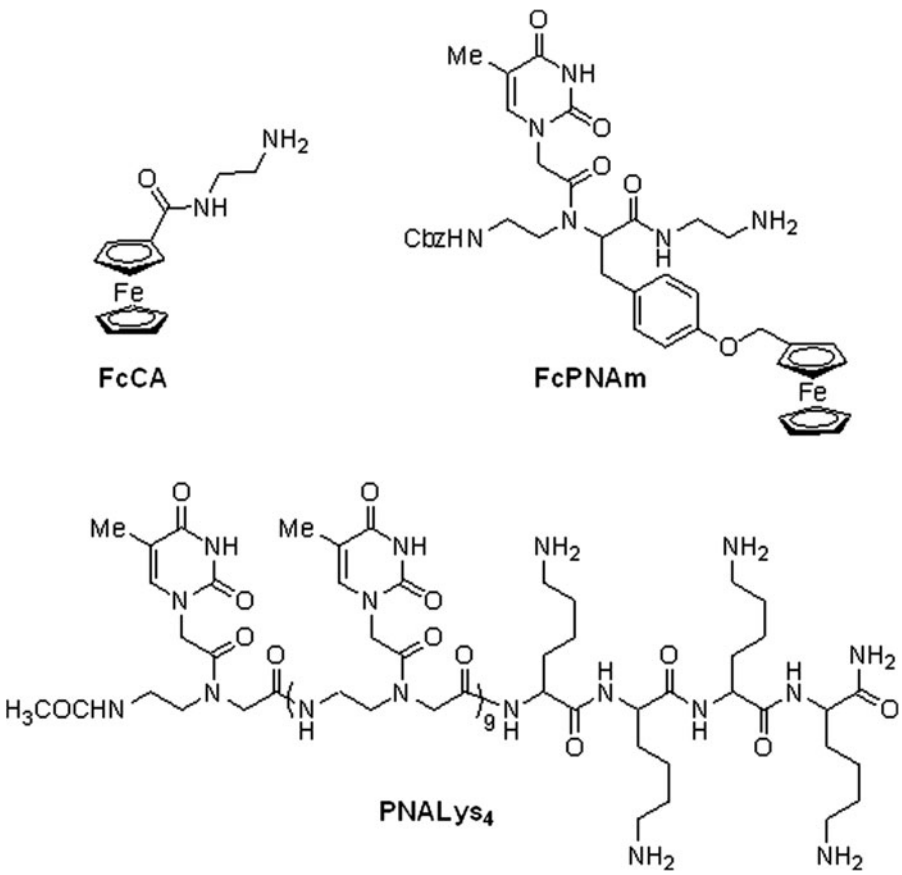

Fig. 1 Molecular probes deposited on the Au surfaces in order to (1) compare the area of the different Au surfaces (FcCA), (2) test the effectiveness of PNA deposition (FcPNAm), and (3) test the effectiveness of Au_{NP} surfaces for high performance amperometric genosensors [PNA(Lys)$_4$]

chemical shifts (δ) are reported in parts per million relative to the solvent peak. Mass spectra were recorded on Advantage Thermo Finnigan instruments (ESI source). IR spectra were recorded on a Perkin Elmer FT-IR 1725X instrument.

Electrochemical tests were performed with an Autolab PGSTAT30 (Ecochemie) potentiostat/galvanostat, equipped with a Metrohm 663 VA stand. The single compartment electrochemical cell consisted of a 2-mm diameter Au disk working electrode (Metrohm), a glassy carbon rod auxiliary electrode (Metrohm), and an aqueous Ag/AgCl, 3 M KCl reference electrode (Amel). Unless otherwise specified, all the potential values given are referred to this reference electrode.

SEM images were acquired using a XL-30 (FEI Company, Oxford Instruments) working in high vacuum conditions. The images of the different surfaces were directly collected on the same substrates used for sensor application. The morphology of the surfaces was investigated by collecting secondary electrons' images using an ETD detector.

TEM images were collected with a JEOL 2010, equipped with energy filter, Gatan Inc. A drop of the AuNP solution was deposited onto a Cu/Formvar/carbon 200 mesh grid. The grid was dried in air for at least 10 min.

UV–Vis spectra of the AuNP solutions were recorded using a Perkin Elmer Lambda 650 spectrophotometer, working in the 180–900 nm spectral range.

Synthesis of molecular probes with an amine terminal group

N-(2-aminoethyl)-ferrocenecarboxyamide (FcCA) was synthesized in 73 % yield as already reported (Liu et al. 2008).

Ferrocene-labeled *N*-(2-aminoethyl)-terminated tyrosine PNA monomer (FcPNAm)—A solution of ferrocene-labeled thymine PNA monomer methyl ester (Baldoli et al. 2004) (120 mg, 0.16 mmol) in CH_2Cl_2 (0.7 mL) was slowly added into pure ethylenediamine (5 mL at 50 °C). The reaction was

completed after stirring for 1 h at 50 °C. After evaporation of the solvent, the residue was taken up with CH_2Cl_2 (10 mL), washed with brine (10 mL), and the aqueous phase was extracted with CH_2Cl_2 (3 × 10 mL). The combined organic phases were washed with water, dried over Na_2SO_4, and evaporated affording FcPNAm as a yellow powder, 115 mg (91 %). m.p. (pentane) 188–189 °C. ^{1}H-NMR ($CDCl_3$) δ (ppm): 1.90 (s, 3H, $-CH_3$, Thymine); 2.70–3.50 (m, 10H, $-NCH_2CH_2N-$, NCH_2CH_2N-, CH_2); 3.8 (m, 1H, CH); 4.01 (s, 1H, C(O)CHN); 4.17 (m, 8H, Fc + C(O)CHN); 4.29 (s, 2H, Fc); 4.75 (s, 2H, $-CH_2-$Fc); 5.05 (m, 2H, $-CH_2-$Ph, Cbz); 6.86 (d, 2H, –OPh); 7.06 (d, 2H, –OPh); 7.25–7.33 (m, 5H, Ph, Cbz). ^{13}C-NMR ($CDCl_3$) δ (ppm): 12.2, 32.9, 39.4, 40.4, 45.6, 49.3, 66.6, 68.5, 69.2, 82.4, 110.4, 115.1, 128.1, 129.1, 129.9, 141.0, 151.3, 157.8, 164.7, 168.4, 170.4. MS (ESI) m/z: 765.2 [M + 1]. FT-IR (Nujol, wavenumber/cm^{-1}): 1665.5 [CONH].

Lysine-terminated homothymine PNA decamer [PNA(Lys)$_4$] was synthesized according to the procedure reported elsewhere (Zanardi et al. 2012).

Synthesis of AuNPs

AuNPs surrounded by chloride ions were synthesized by slightly modifying a procedure previously developed by us (Zanardi et al. 2009). In this case, two aliquots (0.150 mL) of 43 mM $NaBH_4$ aqueous solution were quickly added to 3 mL of 1 mM $NaAuCl_4$ aqueous solution under vigorous stirring; the interval time between the two additions of the reductant was 10 min. The synthesis was allowed to proceed at room temperature for 20 min.

The mean diameter of the AuNPs was calculated from the TEM images (see Fig. 2). They revealed that the AuNPs are characterized by a mean diameter of 3.5 and a 0.9 nm standard deviation. The synthesis of AuNPs was repeated daily and the reproducibility of the synthetic procedure was checked by registering the UV–Vis spectra of the AuNP solutions. A plasmon band, always centered at 515 nm, indicates the high reproducibility degree of the synthetic procedure.

Preparation of Au surfaces

Different gold surfaces have been prepared and compared: (1) smooth Au (Au_{sm}) used just at the end of the cleaning procedure, (2) Au nanostructured through an electrochemical approach (Au_{el}) performed on Au_{sm}, and (3) Au nanostructured by depositing the chemically synthesized AuNPs on Au_{sm} (Au_{NP}). In all cases, the bare Au surface was previously cleaned with piranha solution and carefully washed with an abundant flux of water. The surface was then mechanically cleaned with 1 and 0.3 μm alumina powder and then rinsed with ultrapure water (18 MΩ cm resistivity) in an ultrasonic bath for 5 min. The procedure was completed by cycling the electrode potential between −0.20 and +1.15 V versus saturated Hg/$HgSO_4$ (Amel) at 0.10 V/s potential scan rate in 0.5 M H_2SO_4 solution.

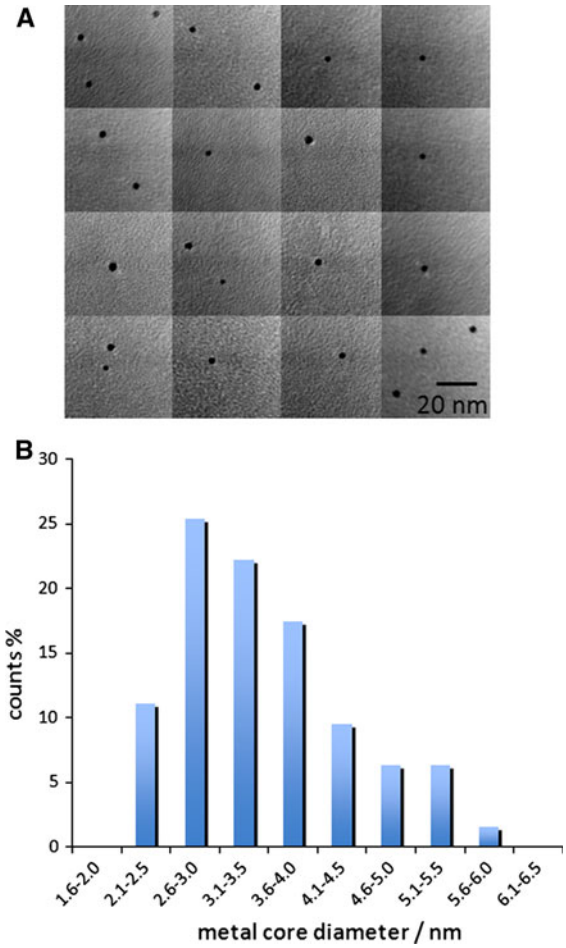

Fig. 2 **A** TEM images of chloride-surrounded AuNPs and **B** a relevant size distribution histogram. Due to the concentration of the AuNP sample, **A** is obtained by merging 16 different images collected on the same TEM grid; no sample concentration was adopted in order to avoid NP aggregation

Au_{el} was obtained by one of the most frequently adopted electrochemical procedure (Fang et al. 2008; Ensafi et al. 2011; Carralero Sanz et al. 2005; Liu et al. 2005; Huang et al. 2008; Zhang et al. 2008). To obtain an Au-nanostructured surface, a Pt counter electrode was coiled around the bare Au electrode and they were both dipped inside a 3 mM $NaAuCl_4$ (Aldrich, 99 %) water solution added with KNO_3 (Riedel-de-Haën, 99 %) to 0.1 M concentration as the supporting electrolyte. The electrode was then polarized at −0.20 V versus Ag/AgCl for 180 s to induce Au(III) electroreduction to Au^0, which precipitates onto the Au surface to form a nanostructure (Mohanty 2011).

Au_{NP} was obtained by a two-step procedure. The Au surface was firstly modified by dipping the electrode in a 10 mM 1,4-benzenedimethanethiol (BDT, Aldrich, 98 % pure) and ethanol solution for 15 min. In the following step, the thiol-modified electrode was dipped in the AuNP solution for 30 min. All the deposition parameters were chosen on the basis of experiments carried out by cyclic voltammetry (CV) in 1 mM $K_4Fe(CN)_6$, phosphate buffer solution (PBS) at pH = 7.0.

Deposition of ferrocene amino derivatives on Au surfaces

The area of the different surfaces, that was active with respect to the deposition of the recognition elements, was compared by depositing FcCA as a probe; the different Au substrates were dipped in a 1 mM ethanol solution at room temperature for different time intervals. The amount of FcCA deposited was evaluated on the basis of the electrochemical signal relative to the oxidation of the ferrocene probe. To this aim, CV experiments were carried out in a 0.05 M tetrabutylammonium hexafluorophosphate ($TBAPF_6$, Aldrich 99.9 + % pure) and $CHCl_3$ solution by scanning the potential between 0.00 and +0.90 V at 0.050 V/s scan rate.

The deposition of FcPNAm onto the Au_{NP} surface was carried out by a similar approach by dipping such a substrate in a 1 mM ethanol solution at room temperature for 30 min.

Sensor building

$PNALys_4$ was deposited onto the Au surface by dipping the electrode in a 0.1 mM, 0.1 M ammonia buffer solution (pH = 10) for 4 h at room temperature. The electrode was then carefully rinsed with abundant ultrapure water and immersed into a 0.1 M PBS solution containing 1 nM of the target oligonucleotide sequence, namely, 5′-AAA-AAAA-AAA-3′, acquired from Primm, Milan (Italy). Hybridization was allowed to proceed at 25 °C for 1 h. The electrode surfaces were finally washed with ultrapure water.

The response of the sensor was tested by registering both CV (0.050 V/s) and SQuare Wave Voltammetric (SQWV—amplitude: 50 mV; frequency: 20 Hz; step potential: 5 mV) signals in 1 mM $K_4Fe(CN)_6$ in PBS before and after the hybridization procedure with the target oligonucleotide sequence. In order to remove molecules not perfectly fixed on the electrode surface, the electrode was rotated for 2 min in PBS at 500 rpm before each voltammetric measurement.

Results and discussion

The new gold-nanostructured surface (Au_{NP}) has been obtained through the stable deposition of chemically synthesized gold nanoparticles onto a gold substrate by means of a dithiol linker, namely 1,4-benzenedimethanethiol (BDT). The performance of the new Au_{NP} surface has been compared with those of smooth Au (Au_{sm}) and Au nanostructured through an electrochemical approach (Au_{el}).

Assembling of Au_{NP} surfaces

The anchoring of BDT molecules on the gold surface has been verified (Finklea 2003; Janek et al. 1998) by the dramatic decrease of the current in the CV traces due to the $K_4Fe(CN)_6$ electroactive probe in solution (see Fig. 3A) and a concurrent increase of the peak potential separation (ΔE). The conditions for BDT deposition have been suitably chosen in order to obtain a high coverage degree of the electrode surface, i.e., a high number of thiol tail groups capable to link AuNPs, in a short time. It is worth noticing that by considering the very short dipping time adopted, a well-ordered BDT self-assembled monolayer structure is far from being reached. In this respect, it was previously checked that the presence of O_2 inside the deposition solution induces the dimerisation of BDT through the formation of disulfide bridge (Pasquali et al. 2007a, b, 2008). The formation of the dimer

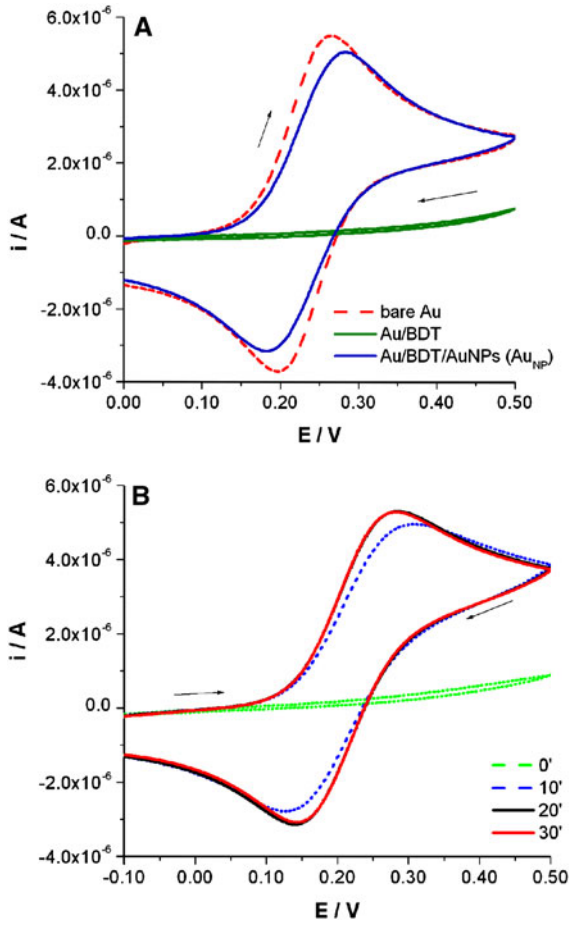

Fig. 3 CV traces registered in 1 mM $[Fe(CN)_6]^{4-}$, 0.1 M PBS **A** in the different phases of Au_{NP} assembly and **B** for different dipping times of the BDT-modified Au surface in AuNP solution. 0.020 V/s potential scan rate

implies the presence of two sulfur atoms suitable to anchor the AuNPs in the "spacer" of the SAM. As a consequence, there is no reason why the deposited AuNPs are only confined in the external region of the organic layer, as schematically sketched in the inset of the SEM image reported in Fig. 4B; rather, is quite possible that a relative disorder characterizes the organic/inorganic deposit.

Further electrochemical tests, carried out after the deposition of AuNPs on the dithiol layer, support this conclusion. Also, in this case, the information concerning the different phases of AuNPs' deposition is collected by registering CV traces due to $[Fe(CN)_6]^{4-/3-}$ redox couple in solution. When AuNPs are deposited on a BDT layer obtained under the previously described experimental

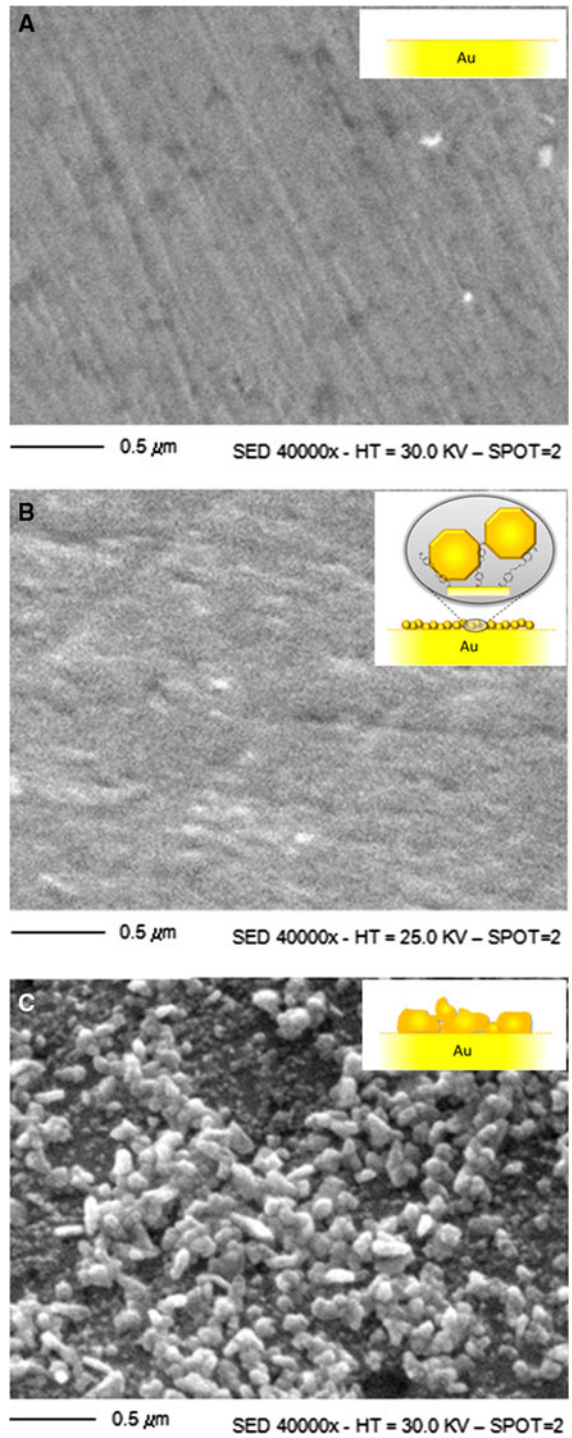

Fig. 4 SEM images of **A** Au_{sm}, **B** Au_{NP}, and **C** Au_{el} obtained from secondary electrons. The *insets* report a schematic representation of the structure of the different gold surfaces as hypothesized on the basis of SEM images and electrochemical data

conditions, a progressive reduction of the charge transfer resistance is observed on increasing the dipping time (see Fig. 3B). As observed, the increasing amount of AuNPs on the electrode surface is found to progressively reduce the charge transfer resistance. Figure 3A reports the voltammetric trace finally registered when AuNPs have been deposited for 30 min, i.e., a time suitable to obtain a steady state voltammogram; the signal finally recalls that which is obtained on a bare Au surface.

A completely different result is evidenced when, on the contrary, BDT coating is realized by prolonging the deposition times overnight. The further deposition of AuNPs on the resulting organic layer only induces a very negligible reduction of charge transfer resistance; the peak-to-peak separation in the CV curves due to $[Fe(CN)_6]^{4-/3-}$ redox couple in solution finally results in ca. 1 V. In this case, we can quite reasonably conclude that the conditions adopted are suitable to allow the organization of a well-defined organic–inorganic bilayer; the compact organic layer induces the confinement of AuNPs only in the external region of the coating, constituting a high resistance to the charge percolation.

In the experimental conditions finally adopted in our case, the shape of the resulting voltammetric trace (Fig. 3A) is consistent with the occurrence of a planar diffusion process; this evidence lets us conclude that the AuNPs on the electrode surface are very close to each other, inducing a total overlap between the diffusion layers of neighboring NPs (Ugo et al. 2002; Moretto et al. 2009; Campbell and Compton 2010). This aspect justifies the fair coincidence of the current values obtained in CV experiments performed with Au_{sm} and with Au_{NP} surfaces, and indicates that a proper evaluation of the gold area available for the deposition of PNA wires is only possible by depositing electrochemical probes on the different surfaces.

The morphology of the resulting nanostructured surface compared to the original smooth one has been studied by the SEM technique. The Au_{sm} image, reported in Fig. 4A, shows a homogeneous morphology characterized by fairly regular scratches due to the mechanical cleaning with alumina powder; the presence of some isolated white grains on the surface is due to residues of alumina. Figure 4B reports one representative image of the Au surface coated with the BDT/AuNP layer. As observed, the wrinkles of the surface are partially leveled out by the presence of the coating. From similar pictures acquired on different zones of the electrode, we can observe that AuNPs are homogeneously distributed on the whole surface, evident segregations being absent. SEM images clearly show the formation of a nanostructured surface characterized by pores possessing dimensions lower than 50 nm, justifying the closeness of the AuNPs to one another.

SEM images of Au_{el} were also acquired in order to compare the two different nanostructures. The morphology of the Au_{el} surface (Fig. 4C) appears quite heterogeneous due to the presence of particles different from one another in both size and shape, and irregularly distributed on the whole surface. As a general consideration, the dimension of the major part of the particles appears of the order of 100 nm, well in agreement with what is reported in the literature (Ensafi et al. 2011; Carralero Sanz et al. 2005). This is a much bigger value than that of Au_{NP} nanostructure, well justifying the different behavior of the two biosensors correspondingly realized, as illustrated henceforth.

Deposition of ferrocene derivatives

As previously discussed, the area of the three different Au surfaces, active with respect to the deposition of the recognition elements, was compared by means of the deposition of an electrochemical redox probe, namely FcCA. The peak intensity due to the reversible oxidation of the ferrocene moiety (i_f) is measured at the different steps of the deposition; as observed in Fig. 5A for deposition on the Au_{NP} surface, it increases on increasing the dipping time, suggesting a progressive increment of the coverage degree of the surface. Figure 5B reports the i_f versus deposition time plot for the three different Au surfaces tested; a nanostructured surface allows the deposition of a higher amount of molecules with respect to Au_{sm}. However, the area suitable for FcCA anchoring is not significantly different in the two different nanostructured surfaces, as suggested by the very similar current values obtained at a 120-min deposition time (see also Table 1). The different morphology of the two nanostructured surfaces, as evidenced by the SEM images, can be related to the different kinetics for FcCA deposition; when Au_{el} is used, i_f increases almost linearly over the whole interval time explored and quite a high amount of molecules are fixed even at the very first steps of the deposition. Although the

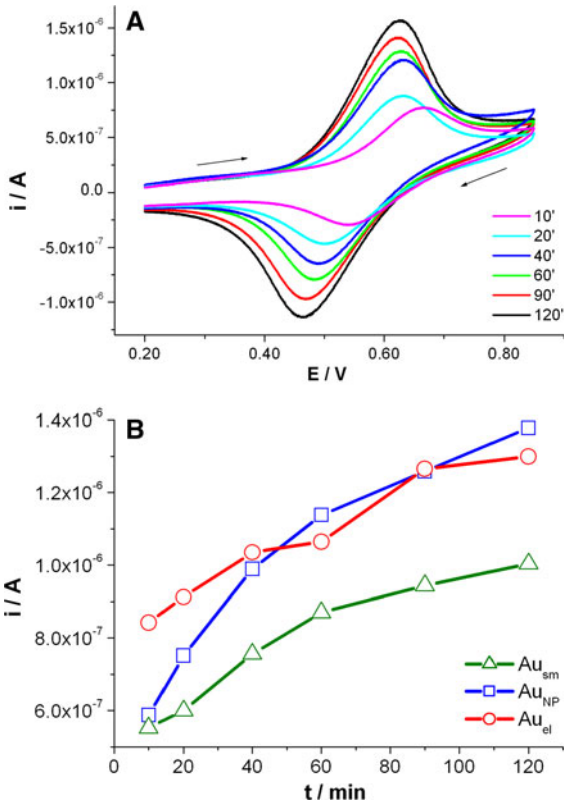

Fig. 5 **A** CV traces at different steps of FcCA deposition on Au_{NP} surface recorded in 0.1 M $TBAPF_6$, $CHCl_3$ solution, 0.050 V/s potential scan rate and **B** the relevant plot of the peak current intensity for Fc residue oxidation versus FcCA deposition time, obtained by CV experiments on the indicated electrode systems; mean values calculated from four different depositions on similar Au surfaces are reported

Table 1 Mean values obtained from four deposition processes of FcCA, carried out on the three Au surfaces

	i_f (μA)	RSD (%)	i_b (μA)	i_f/i_b
Au_{sm}	1.00	5.03	0.48	2.10
Au_{el}	1.30	16.6	0.46	2.80
Au_{NP}	1.38	13.2	0.27	5.01

different behaviors of Au_{el} and Au_{sm} are well evident from the first stages of FcCA deposition, the differences between Au_{NP} and Au_{sm} are more evident the longer the deposition time.

The Relative Standard Deviation (RSD) of the peak current registered after a 120-min FcCA deposition on the different electrodes (Table 1) has been calculated from four depositions in order to test the reproducibility of the nanostructure formation. Although, as expected, the deposition of FcCA on nanostructured surfaces is less reproducible than on the bare Au_{sm} surface, the process can be finally considered well reproducible. This aspect is most important when proposing this system in the frame of disposable sensors.

As a final consideration, we have analyzed the ratios between the faradic current due to oxidation of the ferrocene groups fixed on the surface (i_f) and the contribution of the background currents, also including the capacitive component (i_b) (see Table 1). In fact, i_b constitutes a noise that negatively affects the accurate evaluation of the analytically useful signal, i.e., of the faradic component. As observed from Table 1, a clearly different behavior is exhibited in this respect by the systems developed on the three different substrates; the best results have been obtained for the Au_{NP} surface because i_b is much lower than for the Au_{el} surface.

In order to test the effectiveness of PNA deposition on Au_{NP} surfaces through the amino terminal groups, FcPNAm has been deposited onto Au_{NP} surface. The presence of the Fc redox probe can give us direct evidence of the stable anchoring of the molecule on the nanostructured surface by very simple and rapid electrochemical tests. The actual anchoring of this PNA monomer on the Au-nanostructured surface has been evidenced by a well-defined voltammetric trace, with $E_{1/2} = 0.55$ V, and by the direct proportionality of $i_{p,a}$ to the potential scan rate (see Fig. 6), which indicates a surface-confined electrochemical process. The very good overlap of all traces of a wide series of

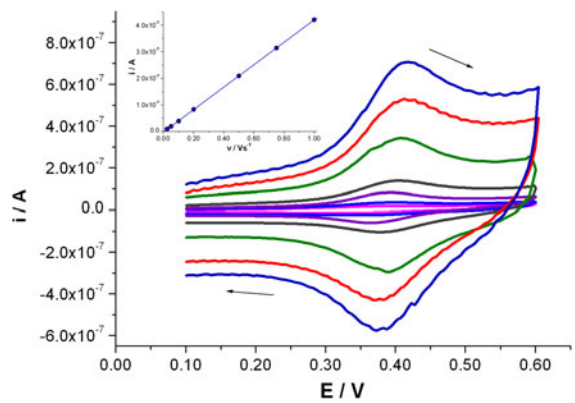

Fig. 6 CV of FcPNAm-modified Au_{NP}-nanostructured surface in 0.1 M $TBAPF_6$ and $CHCl_3$ solvent media at different scan rates. The trend of $i_{p,a}$ versus potential scan rate (0.025–1.000 V/s) is reported in the *inset*

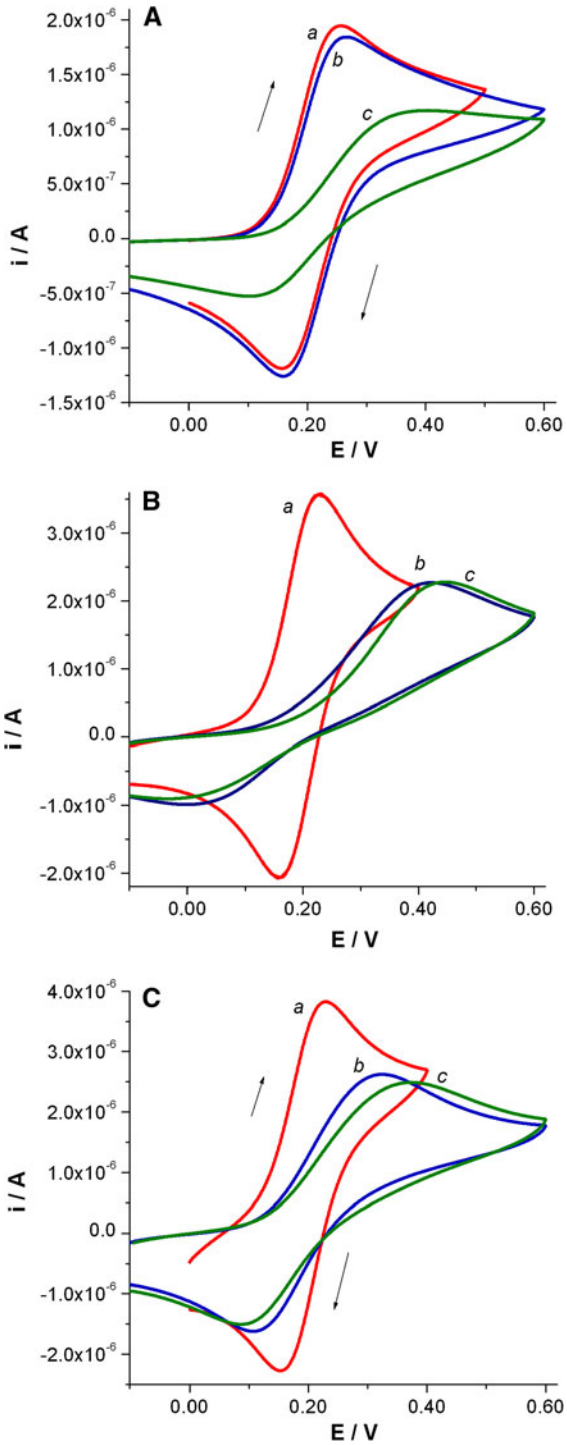

Fig. 7 CV traces of **A** Au_{NP}, **B** Au_{sm}, and **C** Au_{el} surfaces in 1 mM $[Fe(CN)_6]^{4-}$, 0.1 M PBS in the different phases of sensing system realization: (*a*) bare Au surfaces, (*b*) after PNA deposition and (*c*) after hybridization with 2 nM solution containing the target oligonucleotide sequence

CV curves recorded at the end of the deposition indicates that the deposition of FcPNAm through the amine terminal group is stable.

Au surfaces as the transducers for amperometric genosensors

$PNA(Lys)_4$ was deposited onto the three examined surfaces in order to test their performances when used for developing genosensors. The actual occurrence of the stable deposition of PNA on gold surfaces was indirectly verified by registering the CV signals relative to $[Fe(CN)_6]^{4-}$ oxidation before and after PNA deposition (see Fig. 7). The slight increment of forward and backward peak potential separation and the very small reduction of the peak intensity evidenced in the case of Au_{NP} surfaces (Fig. 7A) are consistent with the presence of a poorly packed non-conductive layer on the surface. On the contrary, when Au_{sm} and Au_{el} surfaces are employed, the features of the CV trace of the redox probe in solution indicate that PNA molecules on the surface form a more tightly packed organic layer (Fig. 7B, C). The close similarity of the CV traces registered with Au_{el} with Au_{sm} surfaces is in agreement with the relevant morphology, reported in Fig. 4; the dimension of Au terraces in the grains obtained through the electrochemical approach may be so large to be quite similar to those in Au_{sm}. In conclusion, electrochemical tests constitute a clear, though indirect, indication that the effect of the underlying gold structure on the orientation of PNA molecules on the surface is very similar in the two cases.

The efficiency of the realized PNA-Au_{NP} electrode system in detecting very low concentrations of the target complementary oligonucleotide sequence has been verified by adopting a label-free amperometric detection method (Aoki et al. 2000; Aoki and Tao 2005; Degefa and Kwak 2008). It exploits of the anionic nature of DNA and RNA strands in contrast to the neutral charge of the PNA structure. The decrement of the current due to the oxidation of the negatively charged electroactive $[Fe(CN)_6]^{4-}$ species, deliberately added to the solution, is related to the negative charge density arising from actual formation of duplexes fixed on the AuNP surface. The CV signals registered with this redox probe in solution before ($i_{p,0}$) and after the hybridization process ($i_{p,f}$) with the target oligonucleotide sequence constitute the

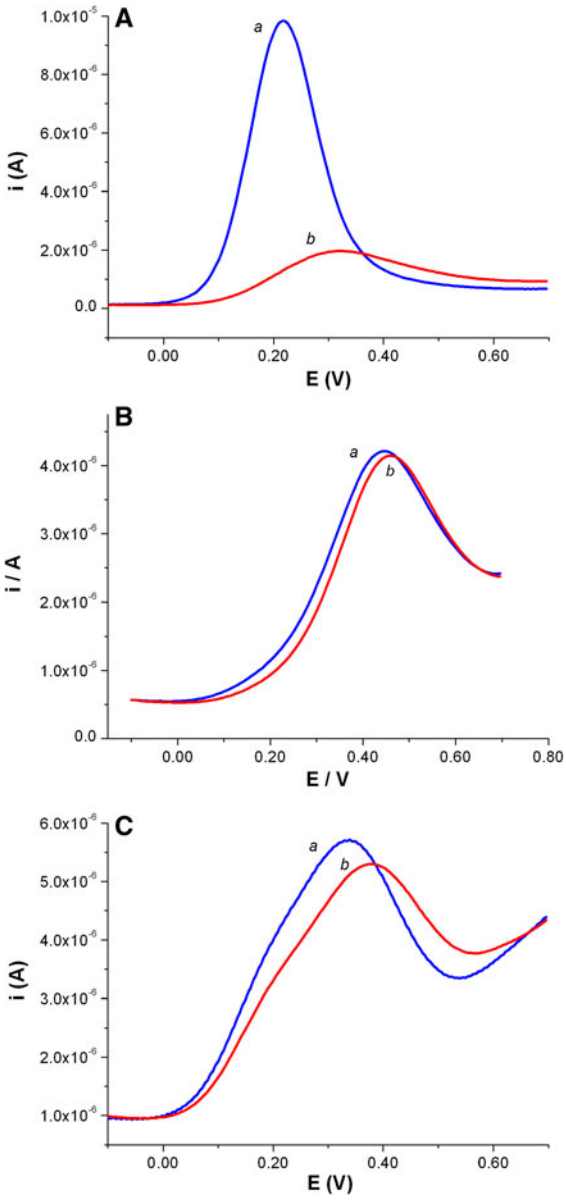

Fig. 8 SQWV traces of **A** Au_{NP}, **B** Au_{sm}, and **C** Au_{el} surfaces in 1 mM $[Fe(CN)_6]^{4-}$, 0.1 M PBS (*a*) before and (*b*) after hybridization with 2 nM solution containing the target oligonucleotide sequence

actual sensor response (Aoki et al. 2000; Aoki and Tao 2005; Degefa and Kwak 2008). Despite the quite low concentration of the target oligonucleotide sequence chosen for these tests (i.e., 2 nM), for all electrode systems, the occurrence of coupling with oligonucleotide molecules induces the arising of a negative cloud adjacent to the electrode and a consequent increase of the charge transfer resistance to the negatively charged probe species. This aspect indicates the effectiveness of PNA in interacting with the target molecule (see Fig. 7).

Table 2 Normalized current decrement obtained before ($i_{p,0}$) and after ($i_{p,f}$) the hybridization process with the target oligonucleotide sequence, obtained from SQWV experiments with sensors built up on different Au surfaces

	$(i_{p,0} - i_{p,f})/i_{p,0} \times 100$ (%)
Au_{sm}	1.5
Au_{el}	18.8
Au_{NP}	80.0

When considering the analytical signal, a more sensitive quantification of the current variation before and after the hybridization process can be obtained from SQWV responses (Fig. 8) since the resulting current is ascribed to faradic reactions, i.e., oxidation process of $[Fe(CN)_6]^{4-}$ in solution, while the contribution of the non-faradic components is minimized. Table 2 reports the current variations registered from SQWV experiments at sensors built up with the three different Au surfaces. As observed, the use of nanostructured surfaces induces more sensitive responses. This effect can be firstly related to the increment of the number of PNA molecules that can be fixed on surfaces possessing larger suitable areas with respect to a smooth one. On the other hand, the extraordinary sensitivity evidenced when using Au_{NP} surfaces leads to conclude that the morphology of the nanostructure plays a key role in the performances of the electrode. As a matter of fact, although preliminary tests with FcCA indicate that the areas of the two nanostructured surfaces are roughly similar, the sensitivity when using the Au_{NP} substrate is incredibly high. In this respect, we have to keep in mind that many amperometric genosensors based on PNA probe molecules, even including those consisting of nanostructured surfaces, show a limit of detection of 1 nM (Won et al. 2008; Aoki and Tao 2005; Fang et al. 2008; Le Floch et al. 2005) that is very close to the concentration value tested with the Au_{NP} surface. We can conclude that the marked curvature of the small AuNPs affects the spatial disposition of PNA chains on the surface, inducing a poorly packed structure that can facilitate the access of oligonucleotide strains to interact with the complementary PNA sequence. These results indicate that the careful control of the substrate morphology constitutes the

basis for the obtainment of a particularly sensitive sensor.

Conclusions

The method proposed for the obtainment of gold-nanostructured surfaces, Au_{NP}, is well reproducible and suitable for stable anchoring PNA strands simply through amine terminal groups. The combination of an enlarged area and, especially, a small curvature radius induced by the presence of small AuNPs allows the detection of 2 nM solution of the target complementary oligonucleotide sequence with very high sensitivity by exploiting a very simple label-free approach. As a matter of fact, preliminary tests carried out on more diluted solutions of the target oligonucleotide sequence demonstrated that the sensor is effective also for concentrations as low as 10 pM. Both sensitivity and detection limits can be further improved by suitably varying the electrochemical probe added to the solution to allow the signal transduction; by following this approach, $[Fe(CN)_6]^{4-}$ can be replaced by multicharged electrochemical probes such as electrochemically active soluble polymers (Le Floch et al. 2005; Fang et al. 2008).

Finally, it is important to underline that similar nanostructured surfaces are also suitable to improve the performances of sensing systems involving different transduction approaches such as the optical and micro-gravimetrical ones.

Acknowledgments Dr. Massimo Tonelli of the Centro Interdipartimentale Grandi Strumenti (CIGS—Università di Modena e Reggio Emilia) is acknowledged for the acquisition of the SEM images. The CIGS is also acknowledged for the use of the TEM instrument. C.Z. and R.S. acknowledge the Ministero dell'Istruzione, dell'Università e della Ricerca (MIUR, Rome) for the financial support from PRIN 2009 (2009YRH27R). E.L. wishes to thank the MIUR (Rome) and the University of Milan for the financial support from PRIN 2007 (2007F9TWKE_002) and PRIN 2009 (20093N774P_003). C.B. wishes to thank CNR-PM.P06.003.

References

Aoki H, Tao H (2005) Trace analysis of an oligonucleotide with a specific sequence using PNA-based ion-channel sensors. Analyst 130:1478–1482

Aoki H, Bühlmann P, Umezawa Y (2000) Electrochemical detection of a one-base mismatch in an oligonucleotide using ion-channel sensors with self-assembled PNA monolayers. Electroanalysis 12:1272–1276

Baldoli C, Falciola L, Licandro E, Maiorana S, Mussini P, Ramani P, Rigamonti C, Zinzalla G (2004) A new ferrocene conjugate of a tyrosine PNA monomer: synthesis and electrochemical properties. J Organomet Chem 689:4791–4802

Bin X, Sargent EH, Kelley SO (2010) Nanostructuring of sensors determines the efficiency of biomolecular capture. Anal Chem 82:5928–5931

Cai H, Xu C, He P, Fang YZ (2001) Colloid Au-enhanced DNA immobilization for the electrochemical detection of sequence-specific DNA. J Electroanal Chem 510:78–85

Campbell FW, Compton RG (2010) The use of nanoparticles in electroanalysis: an updated review. Anal Bioanal Chem 396:241–259

Carralero Sanz V, Luz Mena M, González-Cortés A, Yánez-Sedeno P, Pingarrón JM (2005) Development of a tyrosinase biosensor based on gold nanoparticles-modified glassy carbon electrodes. Application to the measurement of a bioelectrochemical polyphenols index in wines. Anal Chim Acta 528:1–8

Castañeda MT, Alegret S, Merkoçi A (2007) Electrochemical sensing of DNA using gold nanoparticles. Electroanalysis 19:743–753

Cederquist KB, Keating CD (2009) Curvature effects in DNA: Au nanoparticle conjugates. ACSNano 3:256–260

D'Agata R, Corradini R, Ferretti C, Zanoli L, Gatti M, Marchelli R, Spoto G (2010) Ultrasensitive detection of non-amplified genomic DNA by nanoparticle-enhanced surface plasmon resonance imaging. Biosens Bioel 25:2095–2100

Degefa TH, Kwak J (2008) Electrochemical impedance sensing of DNA at PNA self assembled monolayer. J Electroanal Chem 612:37–41

Ensafi AA, Taei M, Rahmani HR, Khayamian T (2011) Sensitive DNA impedance biosensor for detection of cancer, chronic lymphocytic leukemia, based on gold nanoparticles/gold modified electrode. Electrochim Acta 56:8176–8183

Erdem A (2007) Nanomaterial-based electrochemical DNA sensing strategies. Talanta 74:318–325

Fang Z, Kelley SO (2009) Direct electrocatalytic mRNA detection using PNA-nanowire sensors. Anal Chem 81:612–617

Fang B, Jiao S, Li M, Qu Y, Jiang X (2008) Label-free electrochemical detection of DNA using ferrocene-containing cationic polythiophene and PNA probes on nanogold modified electrodes. Biosens Bioel 23:1175–1179

Finklea HO (2003) Electrochemistry of organized monolayers of thoils and related molecules on electrodes. In: Bard A, Robinstein I (eds) Electroanalytical chemistry, vol 19. Marcel Dekker, New York, pp 109–335

Gasparac R, Taft BJ, Lapierre-Devlin MA, Lazarek AD, Xu JM, Kelley SO (2004) Ultrasensitive electrocatalytic DNA detection at two- and three-dimensional nanoelectrodes. J Am Chem Soc 126:12270–12271

Hejazi MS, Pournaghi-Azar MH, Alipour E, Abdolahinia ED, Arami S, Navvah H (2011) Development of a novel electrochemical biosensor for detection and discrimination of DNA sequence and single base mutation in dsDNA samples based on PNA-dsDNA hybridization—a new platform technology. Electroanalysis 23:503–511

Hill HD, Millstone JE, Banholzer MJ, Mirkin CA (2009) The role radius of curvature plays in thiolated oligonucleotide loading on gold nanoparticles. ACSNano 3:418–424

Huang X, Li Y, Chen Y, Wang L (2008) Electrochemical determination of nitrite and iodate by use of gold nanoparticles/poly(3-methylthiophene) composites coated glassy carbon electrode. Sens Act B 134:780–786

Janek RP, Fawcett WR, Ulman A (1998) Impedance spectroscopy of self-assembled monolayers on Au(111): sodium ferrocyanide charge transfer at modified electrodes. Langmuir 14:3011–3018

Le Floch F, Ho H, Harding-Lepage P, Bédard M, Neagu-Plesu R, Leclerc M (2005) Ferrocene-functionalized cationic polythiophene for the label-free electrochemical detection of DNA. Adv Mater 17:1251–1254

Li D, Song S, Fan C (2010) Target-responsive structural switching for nucleic acid-based sensors. Acc Chem Res 43:631–641

Li Z, Zhu Z, Liu W, Zhou Y, Han B, Gao Y, Tang Z (2012) Reversible plasmonic circular dichroism of Au nanorod and DNA assemblies. J Am Chem Soc 134:3322–3325

Liu S, Li Y, Li J, Jiang L (2005) Enhancement of DNA immobilization and hybridization on gold electrode modified by nanogold aggregates. Biosens Bioel 21:789–795

Liu J, He P, Yan J, Fang X, Peng J, Liu K, Fang Y (2008) An organometallic super-gelator with multiple-stimulus responsive properties. Adv Mater 20:2508–2511

Lord H, Kelley SOJ (2009) Nanomaterials for ultrasensitive electrochemical nucleic acids biosensing. Mater Chem 19:3127–3134

Mateo-Martí E, Pradier C (2010) A novel type of nucleic acid-based biosensors: the use of PNA probes, associated with surface science and electrochemical detection techniques. In: Somerset VS (ed) Intelligent and biosensors. InTech, Open Access Publisher, USA, pp 323–344

Merkoçi A (2010) Nanoparticles-based strategies for DNA, protein and cell sensors. Biosens Bioel 26:1164–1177

Mohanty US (2011) Electrodeposition: a versatile and inexpensive tool for the synthesis of nanoparticles, nanorods, nanowires, and nanoclusters of metals. J Appl Electrochem 41:257–270

Moretto L, Panero S, Scrosati B, Ugo P (2009) Template ensemble of nanoelectrodes. In: Lin Y, Nalwa HS (eds) Handbook of electrochemical technology, vol 1. American Scientific Publisher, California, pp 87–105

Nielsen PE (2004) Peptide nucleic acids: protocols and applications, 2nd edn. Horizon Bioscience, Wymondham

Oh B, Choi J (2010) Application of peptide nucleic acid towards development of nanobiosensor arrays. Bioelectrochemistry 79:153–161

Pasquali L, Terzi F, Zanardi C, Pigani L, Seeber R, Paolicelli G, Suturin SM, Mahne N, Nannarone S (2007a) Structure and properties of 1,4-benzenedimethanethiol films grown from solution on Au(111): an XPS and NEXAFS study. Surf Sci 601:1419–1427

Pasquali L, Terzi F, Zanardi C, Seeber R, Paolicelli G, Mahne N, Nannarone S (2007b) Bonding and orientation of 1,4-benzenedimethanethiol on Au(111) prepared from solution and from gas phase. J Physics C 19:305020

Pasquali L, Terzi F, Seeber R, Doyle BP, Nannarone S (2008) Adsorption geometry variation of 1,4-benzenedimethanethiol SAMs on Au(111) grown from the vapour phase. J Chem Phys 128:134711–134721

Pasquali L, Terzi F, Seeber R, Nannarone S, Datta D, Dablemont C, Hamoudi H, Canepa M, Esaulov A (2011) A UPS, XPS and NEXAFS study of self-assembly of standing 1,4-benzenedimethanethiol SAMs on gold. Langmuir 27: 4713–4720

Pournaghi-Azar MH, Ahour F, Hejazi MS (2010) Direct detection and discrimination of double-stranded oligonucleotide corresponding to hepatitis C virus genotype 3a using an electrochemical DNA biosensor based on peptide nucleic acid and double-stranded DNA hybridization. Anal Bioanal Chem 397:3581–3587

Rosi NL, Mirkin CA (2005) Nanostructures in biodiagnostics. Chem Rev 105:1547–1562

Salah KA, Alrokyan SA, Khan MN, Ansar AA (2010) Nanomaterials as analytical tools for genosensors. Sensors 10:963–993

Sforza S, Corradini R, Tedeschi T, Marchelli R (2011) Food analysis and food authentication by peptide nucleic acid (PNA)-based technologies. Chem Soc Rev 40:221–232

Soleymani L, Fang Z, Sun X, Yang H, Taft BJ, Sargent EH, Kelley SO (2009) Nanostructuring of patterned microelectrodes to enhance the sensitivity of electrochemical nucleic acids detection. Angew Chem Int Ed 48:8457–8460

Soreta TR, Henry OYF, OïSullivan CK (2011) Electrode surface nanostructuring via nanoparticle electronucleation for signal enhancement in electrochemical genosensors. Biosens Bioel 26:3962–3966

Ugo P, Moretto L, Vezzà F (2002) Ionomer-coated electrodes and nanoelectrode ensembles as electrochemical environmental sensors: recent advances and prospects. ChemPhysChem 3:917–925

Vernille JP, Kovell LC, Schneider JW (2004) Peptide nucleic acid (PNA) amphiphiles: synthesis, self-assembly, and duplex stability. Bioconj Che. 15:1314–1321

Wang J (2005) Nanomaterial-based electrochemical biosensors. Analyst 130:421–426

Wang J, Gong J, Xiong Y, Yang J, Gao Y, Liu Y, Lu X, Tang Z (2011a) Shape-dependent electrocatalytic activity of monodispersed gold nanocrystals toward glucose oxidation. Chem Commun 47:6894–6896

Wang L, Chen X, Wang X, Han X, Liu S, Zhao C (2011b) Electrochemical synthesis of gold nanostructure modified electrode and its development in electrochemical DNA biosensor. Biosens Bioel 30:151–157

Won BY, Yoon HC, Park HG (2008) Enzyme-catalyzed signal amplification for electrochemical DNA detection with a PNA-modified electrode. Analyst 133:100–104

Zanardi C, Terzi F, Zanfrognini B, Pigani L, Seeber R, Lukkeri J, Aaritalo T (2009) Effective electrocatalytic system based on polyviologen and Au nanoparticles multilayer. Sens Act B 144:92–98

Zanardi C, Terzi F, Seeber R, Baldoli C, Licandro E, Maiorana S (2012) Peptide nucleic acid tagged with four lysine residues for amperometric genosensors. Artificial DNA 3:80–87

Zhang K, Ma H, Zhang L, Zhang Y (2008) Fabrication of a sensitive impedance biosensor of DNA hybridization based on gold nanoparticles modified gold electrode. Electroanalysis 20:2127–2133